# Flavour Independent Search for Neutral Higgs Bosons at LEP

The L3 Collaboration

## Abstract

A flavour independent search for the CP-even and CP-odd neutral Higgs bosons h and A is performed in 624 pb$^{-1}$ of data collected with the L3 detector at LEP at centre-of-mass energies between 189 and 209 GeV. Higgs boson production through the $e^+e^- \rightarrow Zh$ and the $e^+e^- \rightarrow hA$ processes is considered and decays of the Higgs bosons into hadrons are studied. No significant signal is observed and 95% confidence level limits on the hZZ and hAZ couplings are derived as a function of the Higgs boson masses. Assuming the Standard Model cross section for the Higgs-strahlung process and a 100% branching fraction into hadrons, a 95% confidence level lower limit on the mass of the Higgs boson is set at 110.3 GeV.

# 1  Introduction

One of the goals of the LEP program is the search for Higgs bosons, the particles postulated by the Standard Model of the electroweak interactions [?], and some of its extensions, to explain the mechanism [?] which gives the elementary particles their observed masses.

At the centre-of-mass energies, $\sqrt{s}$, at which the LEP $e^+e^-$ collider was operated, the Standard Model Higgs boson, H, is predicted to decay dominantly into b quarks. For a large part of the parameter space of the Minimal Supersymmetric Standard Model (MSSM) [?], decays of neutral Higgs bosons into b quarks are also predicted to be dominant. Experimental searches for the Higgs bosons predicted both in the Standard Model and in the MSSM exploit this feature through sophisticated flavour tagging techniques. No significant signal was found at LEP either for the Standard Model Higgs boson [?, ?, ?, ?] or for neutral Higgs bosons of the MSSM [?, ?, ?].

In some extensions of the Standard Model, decays of the Higgs bosons into $b\bar{b}$ pairs are strongly suppressed to the benefit of other decay modes such as $c\bar{c}$, gg or $\tau^+\tau^-$. For instance, this occurs for specific parameters of the two Higgs doublet model [?] or the MSSM [?], as well as for some composite models [?]. It is hence important to investigate such scenarios with dedicated experimental analyses in which the information about the flavour of the Higgs boson decay products is not used, reducing the model dependence of the conventional Higgs searches.

This Letter describes the search for hadronic decays of the light CP-even Higgs boson, h, and of the CP-odd Higgs boson, A, using data collected by the L3 detector [?] at LEP. Production of a h boson in association with a Z boson, Higgs-strahlung, and pair-production of the h and A bosons, are considered:

$$e^+e^- \to hZ, \quad e^+e^- \to hA.$$

The tree level cross sections of these processes are related to the cross section of the Standard Model Higgs boson production through the Higgs-strahlung process, $\sigma_{\mathrm{HZ}}^{\mathrm{SM}}$, as [?]:

$$\sigma_{\mathrm{hZ}} = \xi^2 \sigma_{\mathrm{HZ}}^{\mathrm{SM}}, \quad \sigma_{\mathrm{hA}} = \eta^2 \tilde{\lambda} \sigma_{\mathrm{HZ}}^{\mathrm{SM}},$$

where $\tilde{\lambda}$ is a p-wave suppression factor, which depends on $\sqrt{s}$ and on the Higgs boson masses, $m_{\mathrm{h}}$ and $m_{\mathrm{A}}$. The hZZ and hAZ couplings relative to the HZZ coupling of the Standard Model are defined as $\xi = g_{\mathrm{hZZ}}/g_{\mathrm{HZZ}}^{\mathrm{SM}}$ and $\eta = g_{\mathrm{hAZ}}/g_{\mathrm{HZZ}}^{\mathrm{SM}}$. In the following, these couplings are not fixed to any prediction but rather considered as free parameters, reducing the model dependence of the analysis.

# 2  Data and Monte Carlo samples

An integrated luminosity of 624 pb$^{-1}$ of data, collected at $\sqrt{s} = 189 - 209$ GeV, is analysed. The data are grouped into several subsamples according to their $\sqrt{s}$ value, as listed in Table 1.

The cross section of the Higgs-strahlung process in the Standard Model is calculated using the HZHA generator [?]. For efficiency studies, Monte Carlo samples are generated using PYTHIA [?] for the two production mechanisms and for each of the decay modes h $\to b\bar{b}$, $c\bar{c}$ and gg, A $\to b\bar{b}$, $c\bar{c}$ and gg. Several Higgs mass hypotheses are considered and 2000 events are generated in each case. For the $e^+e^- \to hZ$ process, $m_{\mathrm{h}}$ ranges in steps of 10 GeV from 60 to 100 GeV, and in steps of 1 GeV from 100 to 120 GeV. For the $e^+e^- \to hA$ process, $m_{\mathrm{h}}$ and $m_{\mathrm{A}}$ range from 40 to 110 GeV in steps of 10 GeV.

For background studies, the following Monte Carlo programs are used: KK2f [?] for $e^+e^- \to q\bar{q}(\gamma)$ and $e^+e^- \to \tau^+\tau^-$, PYTHIA for $e^+e^- \to ZZ$ and $e^+e^- \to Ze^+e^-$ and YFSWW [?] for $e^+e^- \to W^+W^-$. EXCALIBUR [?] is used for four-fermion final states not covered by these generators. Hadron production in two-photon interactions is simulated with PYTHIA and PHOJET [?]. The number of simulated events for the most important background channels is more than 100 times the number of expected events.

The L3 detector response is simulated using the GEANT program [?], which models the effects of energy loss, multiple scattering and showering in the detector. The GHEISHA program [?] is used to simulate hadronic interactions. Time dependent detector inefficiencies, monitored during data taking, are also taken into account.

# 3    Analysis procedures

Three different decay modes are considered for the h and A bosons: $b\bar{b}$, $c\bar{c}$ and gg. Table 2 summarises the different signal signatures and the investigated topologies. Three topologies cover the possible final states of the $e^+e^- \to hZ$ process. They correspond to the decay of the Z boson into hadrons, neutrinos or charged leptons, associated to the hadrons from the h decay. They give rise to events with four hadronic jets, two hadronic jets and missing energy and two hadronic jets and two charged leptons, respectively. A single topology consisting of four hadronic jets, covers all final states of the $e^+e^- \to hA$ process.

Analyses in all channels proceed from a preselection of high multiplicity hadronic events which suppresses copious backgrounds from two-photon interactions, lepton-pair production and pair-production of gauge bosons which decay into leptons. A selection based on kinematic cuts, neural networks or likelihoods is then applied to further discriminate the signal from the background. Finally, discriminant variables which depend on the Higgs mass hypothesis are built to separate signal and background. Their distributions are studied to test the presence of a signal and to probe the $\xi$ and $\eta$ couplings as a function of $m_h$ and $m_A$. Events are ordered as a function of the signal over background ratio and only events with this ratio greater than 0.05 are retained.

# 4    Search for $e^+e^- \to hZ$

The three analyses used in the search for $e^+e^- \to hZ$ are similar to those used in the search for the Standard Model Higgs boson [?], with the exception that no b quark identification is used.

## 4.1    Four jets

If both the h and the Z bosons decay into hadrons, the signature is four hadronic jets. The invariant mass of two of them has to be compatible with the mass of the Z boson, $m_Z$. The dominant background comes from hadronic decays of pair-produced gauge bosons and from the $e^+e^- \to q\bar{q}(\gamma)$ process.

After a preselection of high multiplicity events [?], events are resolved into four jets using the DURHAM algorithm [?] and a kinematic fit imposing four-momentum conservation is performed. A likelihood, $L_{hZ}$, is built [?] from the following variables:

- the maximum energy difference between any two jets,

- the minimum jet energy,

- the parameter $y_{34}$ of the DURHAM algorithm for which the event is resolved from three into four jets,

- the minimum opening angle between any two jets,

- the event sphericity,

- the absolute value of the cosine of the polar angle, $\Theta_{2B}$, for the di-jet system most compatible with the production of a pair of gauge bosons,

- the mass from a kinematic fit imposing four-momentum conservation and equal di-jet masses, $m_{5C}$,

- the maximal triple-jet boost, $\gamma_{\text{triple}}$, defined as the maximum three-jet boost obtained from the four possibilities to construct a one-jet against three-jet configuration in a four-jet event.

Figure 1 shows the distributions of $|\cos\Theta_{2B}|$, $m_{5C}$, $\gamma_{\text{triple}}$ and $L_{hZ}$ for data collected at $\sqrt{s} > 203$ GeV, the expected background and a signal with $m_h = 110$ GeV. Events are retained for which the value of $L_{hZ}$ exceeds a threshold, around 0.6, optimised separately for each $\sqrt{s}$ and $m_h$ hypothesis.

For each of the three possible jet pairings, the quantity $\chi^2_{hZ} = \left(\Sigma - (m_h + m_Z)\right)^2/\sigma^2_\Sigma + \left(\Delta - |m_h - m_Z|\right)^2/\sigma^2_\Delta$ is calculated [?], where $\Sigma$ and $\Delta$ are the di-jet mass sum and difference, while $\sigma_\Sigma$ and $\sigma_\Delta$ are the corresponding resolutions. The pairing which minimises $\chi^2_{hZ}$ is chosen and the corresponding value is used as the final discriminant variable. Figure 2a presents the distributions of the signal over background ratio in the $\chi^2_{hZ}$ variable for selected data and Monte Carlo events. Table 3 lists the numbers of selected and expected events for different $m_h$ hypotheses.

## 4.2 Two jets and missing energy

The signature for h decays into hadrons and Z decays into neutrinos is a pair of high multiplicity jets, large missing energy and a missing mass, $m_{\text{mis}}$, consistent with $m_Z$. The dominant backgrounds are the $e^+e^- \rightarrow q\bar{q}(\gamma)$ process, W pair-production in which only one W decays into hadrons and Z pair-production with a Z decaying into hadrons and the other into neutrinos.

High multiplicity hadronic events are selected with a visible energy, $E_{\text{vis}}$, such that $0.25 < E_{\text{vis}}/\sqrt{s} < 0.70$. Events with isolated photons of energy greater than 20 GeV are rejected. The events are forced into two jets using the DURHAM algorithm and the di-jet mass is required to be greater than 40 GeV to suppress background from two-photon interactions. Events from the $e^+e^- \rightarrow q\bar{q}(\gamma)$ process are suppressed by requiring $m_{\text{mis}} > 60$ GeV. In addition, the polar angle, $\theta$, of the missing momentum must satisfy $|\cos\theta| < 0.9$ and the energy deposited in the very forward calorimeters is required to be less than 20 GeV. Finally, the sine of the angle $\Psi$ between the beam axis and the plane spanned by the directions of the two jets must be greater than 0.025. Figures 3a and 3b present the distributions of $m_{\text{mis}}$ and $\sin\Psi$ for data collected at $\sqrt{s} > 203$ GeV, expected background and a signal with $m_h = 110$ GeV, when all other cuts are applied.

A neural network [?] is built from the following variables:

- $E_{vis}$,

- $m_{mis}$,

- $\sin \Psi$,

- the longitudinal missing momentum,

- the transverse missing momentum,

- the absolute value of the cosine of the angle between the two jets in the plane transverse to the beam direction,

- the event thrust,

- the sum of the jet opening angles after forcing the event into a three-jet configuration.

The distributions of the output of the neural network are presented in Figure 3c. Figure 3d shows the distributions of the hadronic mass $m_{qq}$, calculated with a fit which imposes $m_{mis} = m_Z$. These two variables are combined into a final discriminant, whose distributions are presented in Figure 2b in terms of the signal over background ratio. Table 3 lists the numbers of selected events for different $m_h$ hypotheses.

## 4.3 Two jets and two leptons

Different signal topologies correspond to h decays into hadrons and Z decays into electrons and muons or into tau leptons. For decays into electrons and muons, the signature is a pair of well isolated leptons with mass close to $m_Z$ and two hadronic jets. In the case of tau leptons, events with four jets are expected, where two of the jets are narrow, of low multiplicity, and of unit charge. The dominant background is due to Z-pair production followed by the hadronic decay of one Z and the decay into leptons of the other.

The event selection is identical to that used for the same final states of the Standard Model Higgs search [?]. After this selection, a kinematic fit is applied which imposes four-momentum conservation and constrains the di-lepton mass to $m_Z$. The mass of the hadronic system after the fit is used as a discriminant to test different $m_h$ hypotheses. Its distributions in terms of the signal over background ratio are presented in Figure 2c. The yield of this selection is presented in Table 3.

# 5 Search for $e^+e^- \rightarrow hA$

The pair-production of h and A bosons gives rise to high multiplicity events with four hadronic jets. The largest backgrounds are the pair-production of W and Z bosons which decay into hadrons and the $e^+e^- \rightarrow q\bar{q}(\gamma)$ process. High multiplicity events are selected, subjected to a kinematic fit which enforces four-momentum conservation and forced into four jets with the DURHAM algorithm. A neural network [?] is used to separate genuine four-jet events from events most likely due to fermion-pair production.

For each $(m_h, m_A)$ hypothesis, a likelihood, $L_{hA}$, is built [?] to separate the signal from the background from W- and Z-pair production. It uses the following variables:

- the maximum energy difference between any two jets,

- the minimum jet energy,

- the probabilities of kinematic fits which impose four-momentum conservation together with the hypotheses of W- or Z-pair production,

- the cosine of the polar angle of the di-jet system which best fits the hA pair-production hypothesis,

- the cosine of the polar angle, $\Theta_{W^+}$, at which the positive charged[1] boson is produced for the di-jet system which best fits the W-pair production hypothesis,

- $y_{34}$,

- the absolute value of the cosine of the polar angle, $\Theta_T$, of the thrust axis.

Figure 4 shows the distributions of the last three variables and of $L_{hA}$ for data, the expected background and the signal corresponding to the Higgs boson mass hypothesis $(m_h, m_A) = (60,80)$ GeV. A cut on $L_{hA}$ is applied, which depends on $\sqrt{s}$ and on the $(m_h, m_A)$ hypothesis, typically around 0.2. The remaining events are tested for consistency with a given $(m_h, m_A)$ hypothesis by means of the variable $\chi^2_{hA}$ [?], defined analogously to $\chi^2_{hZ}$. The pairing which minimises the value of $\chi^2_{hA}$ is chosen. For each event and each $(m_h, m_A)$ hypothesis, the value of the signal over background ratio of the variable $\chi^2_{hA}$ is calculated. The distributions of these ratios are presented in Figure 5 for different mass hypotheses.

Table 4 reports the numbers of observed events, expected background and expected signal events for several Higgs boson mass hypotheses, together with selection efficiencies.

# 6   Results

Table 3 shows the result of the combination of the different channels of the $e^+e^- \rightarrow hZ$ search. The observed number of events agrees with the Standard Model expectations. No significant excess is observed either in the $e^+e^- \rightarrow hZ$ search or in the $e^+e^- \rightarrow hA$ search, which is summarised in Table 4. Limits on the $\xi$ and $\eta$ couplings are extracted as a function of $m_h$ and $m_A$ from the distributions of the signal over background ratios derived from the final discriminant variables. The log-likelihood ratio technique [?] is used for the combination of the different channels of the $e^+e^- \rightarrow hZ$ search and to derive all the limits. For each final state, among the three possible decays of the h and A bosons into $b\bar{b}$, $c\bar{c}$ and gg, the case with the lowest efficiency is considered.

Several sources of systematic uncertainties are investigated and their impact on the signal efficiency and the determination of the background level is assesed. The limited Monte Carlo statistics affects the signal by around 2% and the background by around 5%, depending on the final state. The selection criteria are varied within the resolution of the corresponding variables yielding an uncertainty from the selection procedure around 2% on the signal and from 3% to 6% on the background. Lepton identification criteria contribute to this source with an additional 1% for the signal and 2% for the background. The expected background level has an uncertainty up to 5%, depending on the final state, due to the uncertainty in the calculation of the cross sections of background processes.

---

[1] Charge assignment is based on jet-charge techniques [?].

Particular care is payed to validate the accuracy of the simulation of gluon jets. A reference sample of three-jet events, from the $e^+e^- \to q\bar{q}g(\gamma)$ process, is selected and the jet with the smallest energy in the rest frame of the hadronic system is taken as the gluon jet. The distributions of the most important gluon jet characteristics such as jet broadening, boosted sphericity and charged track multiplicity are compared for data and Monte Carlo samples. The latter, for instance, is found to be on average overestimated by the simulations and is not considered as input to the likelihoods and the neural networks. From this comparison, an additional systematic uncertainty is assigned as 1.5% for the signal and 2% for the background.

The overall systematic uncertainties depend on the search channel and are estimated to range between 2% and 4% for the signal efficiencies and between 4% and 8% for the background levels. They are included in the derivation of the limits. For $\xi^2 = 1$ they lower the sensitivity to $m_h$ by about 0.8 GeV and for $\eta^2 = 1$ and $m_h = m_A$ by about 0.7 GeV.

Figure 6 shows the 95% confidence level (CL) upper limit on $\xi^2 \times B(h \to hadrons)$ as a function of $m_h$. The expected limit and the 68.3% and 95.4% probability bands expected in the absence of a signal are also displayed and denoted as $1\sigma$ and $2\sigma$, respectively. For $\xi^2 \times B(h \to hadrons) = 1$, *i.e.* for a cross section equivalent to the Standard Model one and a Higgs boson decaying into hadrons, a 95% CL lower limit of 110.3 GeV is set on $m_h$. The expected limit is 108.7 GeV.

Figure 7 shows the 95% CL upper limit on $\eta^2 \times B(hA \to hadrons)$ as a function of $m_h + m_A$ for several values of $|m_h - m_A|$. The expected limits and the $1\sigma$ and $2\sigma$ probability bands in absence of a signal are also shown. The observed limits for $\eta = 1$ are between 120 and 140 GeV, as expected. An excess of $2.9\sigma$ is observed arond 135 GeV for the $m_h = m_A$ hypothesis. A similar behaviour is also observed in the search for charged Higgs bosonse [?]. This excess is mainly due to data at low values of $\sqrt{s}$. At higher energies and for larger integrated luminosities it does not scale with the cross section expected for a $e^+e^- \to hA$ signal. It is hence ascribed to a statistical fluctuation.

In conclusion, a flavour independent search for h and A bosons produced through Higgsstrahlung or in pairs and decaying into hadrons, shows no evidence of a signal and further constrains the scenario of Higgs bosons light enough to have been produced at LEP.

## The L3 Collaboration:

P.Achard,[20] O.Adriani,[17] M.Aguilar-Benitez,[24] J.Alcaraz,[24] G.Alemanni,[22] J.Allaby,[18] A.Aloisio,[28] M.G.Alviggi,[28] H.Anderhub,[46] V.P.Andreev,[6,33] F.Anselmo,[8] A.Arefiev,[27] T.Azemoon,[3] T.Aziz,[9] P.Bagnaia,[38] A.Bajo,[24] G.Baksay,[25] L.Baksay,[25] S.V.Baldew,[2] S.Banerjee,[9] Sw.Banerjee,[4] A.Barczyk,[46,44] R.Barillère,[18] P.Bartalini,[22] M.Basile,[8] N.Batalova,[43] R.Battiston,[32] A.Bay,[22] F.Becattini,[17] U.Becker,[13] F.Behner,[46] L.Bellucci,[17] R.Berbeco,[3] J.Berdugo,[24] P.Berges,[13] B.Bertucci,[32] B.L.Betev,[46] M.Biasini,[32] M.Biglietti,[28] A.Biland,[46] J.J.Blaising,[4] S.C.Blyth,[34] G.J.Bobbink,[2] A.Böhm,[1] L.Boldizsar,[12] B.Borgia,[38] S.Bottai,[17] D.Bourilkov,[46] M.Bourquin,[20] S.Braccini,[20] J.G.Branson,[40] F.Brochu,[4] J.D.Burger,[13] W.J.Burger,[32] X.D.Cai,[13] M.Capell,[13] G.Cara Romeo,[8] G.Carlino,[28] A.Cartacci,[17] J.Casaus,[24] F.Cavallari,[38] N.Cavallo,[35] C.Cecchi,[32] M.Cerrada,[24] M.Chamizo,[20] Y.H.Chang,[48] M.Chemarin,[23] A.Chen,[48] G.Chen,[7] G.M.Chen,[7] H.F.Chen,[21] H.S.Chen,[7] G.Chiefari,[28] L.Cifarelli,[39] F.Cindolo,[8] I.Clare,[13] R.Clare,[37] G.Coignet,[4] N.Colino,[24] S.Costantini,[38] B.de la Cruz,[24] S.Cucciarelli,[32] J.A.van Dalen,[30] R.de Asmundis,[28] P.Déglon,[20] J.Debreczeni,[12] A.Degré,[4] K.Dehmelt,[25] K.Deiters,[44] D.della Volpe,[28] E.Delmeire,[20] P.Denes,[36] F.DeNotaristefani,[38] A.De Salvo,[46] M.Diemoz,[38] M.Dierckxsens,[2] C.Dionisi,[38] M.Dittmar,[46] A.Doria,[28] M.T.Dova,[10,♯] D.Duchesneau,[4] M.Duda,[1] B.Echenard,[20] A.Eline,[18] A.El Hage,[1] H.El Mamouni,[23] A.Engler,[34] F.J.Eppling,[13] P.Extermann,[20] M.A.Falagan,[24] S.Falciano,[38] A.Favara,[31] J.Fay,[23] O.Fedin,[33] M.Felcini,[46] T.Ferguson,[34] H.Fesefeldt,[1] E.Fiandrini,[32] J.H.Field,[20] F.Filthaut,[30] P.H.Fisher,[13] W.Fisher,[36] I.Fisk,[40] G.Forconi,[13] K.Freudenreich,[46] C.Furetta,[26] Yu.Galaktionov,[27,13] S.N.Ganguli,[9] P.Garcia-Abia,[24] M.Gataullin,[31] S.Gentile,[38] S.Giagu,[38] Z.F.Gong,[21] G.Grenier,[23] O.Grimm,[46] M.W.Gruenewald,[16] M.Guida,[39] R.van Gulik,[2] V.K.Gupta,[36] A.Gurtu,[9] L.J.Gutay,[43] D.Haas,[5] D.Hatzifotiadou,[8] T.Hebbeker,[1] A.Hervé,[18] J.Hirschfelder,[34] H.Hofer,[46] M.Hohlmann,[25] G.Holzner,[46] S.R.Hou,[48] Y.Hu,[30] B.N.Jin,[7] L.W.Jones,[3] P.de Jong,[2] I.Josa-Mutuberría,[24] D.Käfer,[1] M.Kaur,[14] M.N.Kienzle-Focacci,[20] J.K.Kim,[42] J.Kirkby,[18] W.Kittel,[30] A.Klimentov,[13,27] A.C.König,[30] M.Kopal,[43] V.Koutsenko,[13,27] M.Kräber,[46] R.W.Kraemer,[34] A.Krüger,[45] A.Kunin,[13] P.Ladron de Guevara,[24] I.Laktineh,[23] G.Landi,[17] M.Lebeau,[18] A.Lebedev,[13] P.Lebrun,[23] P.Lecomte,[46] P.Lecoq,[18] P.Le Coultre,[46] J.M.Le Goff,[18] R.Leiste,[45] M.Levtchenko,[26] P.Levtchenko,[33] C.Li,[21] S.Likhoded,[45] C.H.Lin,[48] W.T.Lin,[48] F.L.Linde,[2] L.Lista,[28] Z.A.Liu,[7] W.Lohmann,[45] E.Longo,[38] Y.S.Lu,[7] C.Luci,[38] L.Luminari,[38] W.Lustermann,[46] W.G.Ma,[21] L.Malgeri,[20] A.Malinin,[27] C.Maña,[24] J.Mans,[36] J.P.Martin,[23] F.Marzano,[38] K.Mazumdar,[9] R.R.McNeil,[6] S.Mele,[18,28] L.Merola,[28] M.Meschini,[17] W.J.Metzger,[30] A.Mihul,[11] H.Milcent,[18] G.Mirabelli,[38] J.Mnich,[1] G.B.Mohanty,[9] G.S.Muanza,[23] A.J.M.Muijs,[2] B.Musicar,[40] M.Musy,[38] S.Nagy,[15] S.Natale,[20] M.Napolitano,[28] F.Nessi-Tedaldi,[46] H.Newman,[31] A.Nisati,[38] T.Novak,[30] H.Nowak,[45] R.Ofierzynski,[46] G.Organtini,[38] I.Pal,[43] C.Palomares,[24] P.Paolucci,[28] R.Paramatti,[38] G.Passaleva,[17] S.Patricelli,[28] T.Paul,[10] M.Pauluzzi,[32] C.Paus,[13] F.Pauss,[46] M.Pedace,[38] S.Pensotti,[26] D.Perret-Gallix,[4] B.Petersen,[30] D.Piccolo,[28] F.Pierella,[8] M.Pioppi,[32] P.A.Piroué,[36] E.Pistolesi,[26] V.Plyaskin,[27] M.Pohl,[20] V.Pojidaev,[17] J.Pothier,[18] D.Prokofiev,[33] J.Quartieri,[39] G.Rahal-Callot,[46] M.A.Rahaman,[9] P.Raics,[15] N.Raja,[9] R.Ramelli,[46] P.G.Rancoita,[26] R.Ranieri,[17] A.Raspereza,[45] P.Razis,[29] D.Ren,[46] M.Rescigno,[38] S.Reucroft,[10] S.Riemann,[45] K.Riles,[3] B.P.Roe,[3] L.Romero,[24] A.Rosca,[45] C.Rosenbleck,[1] S.Rosier-Lees,[4] S.Roth,[1] J.A.Rubio,[18] G.Ruggiero,[17] H.Rykaczewski,[46] A.Sakharov,[46] S.Saremi,[6] S.Sarkar,[38] J.Salicio,[18] E.Sanchez,[24] C.Schäfer,[18] V.Schegelsky,[33] H.Schopper,[47] D.J.Schotanus,[30] C.Sciacca,[28] L.Servoli,[32] S.Shevchenko,[31] N.Shivarov,[41] V.Shoutko,[13] E.Shumilov,[27] A.Shvorob,[31] D.Son,[42] C.Souga,[23] P.Spillantini,[17] M.Steuer,[13] D.P.Stickland,[36] B.Stoyanov,[41] A.Straessner,[20] K.Sudhakar,[9] G.Sultanov,[41] L.Z.Sun,[21] S.Sushkov,[1] H.Suter,[46] J.D.Swain,[10] Z.Szillasi,[25,¶] X.W.Tang,[7] P.Tarjan,[15] L.Tauscher,[5] L.Taylor,[10] B.Tellili,[23] D.Teyssier,[23] C.Timmermans,[30] Samuel C.C.Ting,[13] S.M.Ting,[13] S.C.Tonwar,[9] J.Tóth,[12] C.Tully,[36] K.L.Tung,[7] J.Ulbricht,[46] E.Valente,[38] R.T.Van de Walle,[30] R.Vasquez,[43] V.Veszpremi,[25] G.Vesztergombi,[12] I.Vetlitsky,[27] D.Vicinanza,[39] G.Viertel,[46] S.Villa,[37] M.Vivargent,[4] S.Vlachos,[5] I.Vodopianov,[25] H.Vogel,[34] H.Vogt,[45] I.Vorobiev,[34,27] A.A.Vorobyov,[33] M.Wadhwa,[5] Q.Wang,[30] X.L.Wang,[21] Z.M.Wang,[21] M.Weber,[1] P.Wienemann,[1] H.Wilkens,[30] S.Wynhoff,[36] L.Xia,[31] Z.Z.Xu,[21] J.Yamamoto,[3] B.Z.Yang,[21] C.G.Yang,[7] H.J.Yang,[3] M.Yang,[7] S.C.Yeh,[49] An.Zalite,[33] Yu.Zalite,[33] Z.P.Zhang,[21] J.Zhao,[21] G.Y.Zhu,[7] R.Y.Zhu,[31] H.L.Zhuang,[7] A.Zichichi,[8,18,19] B.Zimmermann,[46] M.Zöller.[1]

1 III. Physikalisches Institut, RWTH, D-52056 Aachen, Germany[§]

2 National Institute for High Energy Physics, NIKHEF, and University of Amsterdam, NL-1009 DB Amsterdam, The Netherlands

3 University of Michigan, Ann Arbor, MI 48109, USA

4 Laboratoire d'Annecy-le-Vieux de Physique des Particules, LAPP,IN2P3-CNRS, BP 110, F-74941 Annecy-le-Vieux CEDEX, France

5 Institute of Physics, University of Basel, CH-4056 Basel, Switzerland

6 Louisiana State University, Baton Rouge, LA 70803, USA

7 Institute of High Energy Physics, IHEP, 100039 Beijing, China[△]

8 University of Bologna and INFN-Sezione di Bologna, I-40126 Bologna, Italy

9 Tata Institute of Fundamental Research, Mumbai (Bombay) 400 005, India

10 Northeastern University, Boston, MA 02115, USA

11 Institute of Atomic Physics and University of Bucharest, R-76900 Bucharest, Romania

12 Central Research Institute for Physics of the Hungarian Academy of Sciences, H-1525 Budapest 114, Hungary[‡]

13 Massachusetts Institute of Technology, Cambridge, MA 02139, USA

14 Panjab University, Chandigarh 160 014, India.

15 KLTE-ATOMKI, H-4010 Debrecen, Hungary[¶]

16 Department of Experimental Physics, University College Dublin, Belfield, Dublin 4, Ireland

17 INFN Sezione di Firenze and University of Florence, I-50125 Florence, Italy

18 European Laboratory for Particle Physics, CERN, CH-1211 Geneva 23, Switzerland

19 World Laboratory, FBLJA Project, CH-1211 Geneva 23, Switzerland

20 University of Geneva, CH-1211 Geneva 4, Switzerland

21 Chinese University of Science and Technology, USTC, Hefei, Anhui 230 029, China[△]

22 University of Lausanne, CH-1015 Lausanne, Switzerland

23 Institut de Physique Nucléaire de Lyon, IN2P3-CNRS,Université Claude Bernard, F-69622 Villeurbanne, France

24 Centro de Investigaciones Energéticas, Medioambientales y Tecnológicas, CIEMAT, E-28040 Madrid, Spain[♭]

25 Florida Institute of Technology, Melbourne, FL 32901, USA

26 INFN-Sezione di Milano, I-20133 Milan, Italy

27 Institute of Theoretical and Experimental Physics, ITEP, Moscow, Russia

28 INFN-Sezione di Napoli and University of Naples, I-80125 Naples, Italy

29 Department of Physics, University of Cyprus, Nicosia, Cyprus

30 University of Nijmegen and NIKHEF, NL-6525 ED Nijmegen, The Netherlands

31 California Institute of Technology, Pasadena, CA 91125, USA

32 INFN-Sezione di Perugia and Università Degli Studi di Perugia, I-06100 Perugia, Italy

33 Nuclear Physics Institute, St. Petersburg, Russia

34 Carnegie Mellon University, Pittsburgh, PA 15213, USA

35 INFN-Sezione di Napoli and University of Potenza, I-85100 Potenza, Italy

36 Princeton University, Princeton, NJ 08544, USA

37 University of Californa, Riverside, CA 92521, USA

38 INFN-Sezione di Roma and University of Rome, "La Sapienza", I-00185 Rome, Italy

39 University and INFN, Salerno, I-84100 Salerno, Italy

40 University of California, San Diego, CA 92093, USA

41 Bulgarian Academy of Sciences, Central Lab. of Mechatronics and Instrumentation, BU-1113 Sofia, Bulgaria

42 The Center for High Energy Physics, Kyungpook National University, 702-701 Taegu, Republic of Korea

43 Purdue University, West Lafayette, IN 47907, USA

44 Paul Scherrer Institut, PSI, CH-5232 Villigen, Switzerland

45 DESY, D-15738 Zeuthen, Germany

46 Eidgenössische Technische Hochschule, ETH Zürich, CH-8093 Zürich, Switzerland

47 University of Hamburg, D-22761 Hamburg, Germany

48 National Central University, Chung-Li, Taiwan, China

49 Department of Physics, National Tsing Hua University, Taiwan, China

| $\sqrt{s}$ (GeV) | 188.6 | 191.6 | 195.6 | 199.5 | 201.5 | 203.8 | 205.1 | 206.3 | 206.6 | 208.0 |
|---|---|---|---|---|---|---|---|---|---|---|
| $\mathcal{L}$ (pb$^{-1}$) | 176.4 | 29.7 | 83.7 | 82.8 | 37.0 | 7.6 | 68.1 | 66.9 | 63.7 | 8.2 |

Table 1: Effective centre-of-mass energies and corresponding integrated luminosities, $\mathcal{L}$.

| Process | | Process | |
|---|---|---|---|
| $e^+e^- \to hZ$ | | $e^+e^- \to hA$ | |
| $h \to b\bar{b}, c\bar{c}, gg \quad Z \to q\bar{q}, \nu\bar{\nu}, \ell^+\ell^-$ | | $h \to b\bar{b}, c\bar{c}, gg \quad A \to b\bar{b}, c\bar{c}, gg$ | |
| Final state | Topology | Final State | Topology |
| $b\bar{b}q\bar{q}, c\bar{c}q\bar{q}, ggq\bar{q}$ | Four jets | $b\bar{b}b\bar{b}, b\bar{b}c\bar{c}$ | |
| $b\bar{b}\nu\bar{\nu}, c\bar{c}\nu\bar{\nu}, gg\nu\bar{\nu}$ | Two jets and missing energy | $b\bar{b}gg, c\bar{c}c\bar{c}$ | Four jets |
| $b\bar{b}\ell^+\ell^-, c\bar{c}\ell^+\ell^-, gg\ell^+\ell^-$ | Two jets and two leptons | $c\bar{c}gg, gggg$ | |

Table 2: Final states of the $e^+e^- \to hZ$ and $e^+e^- \to hA$ processes and topologies under study.

| $e^+e^- \to hZ$ | | | | | | | | |
|---|---|---|---|---|---|---|---|---|
| | $h \to$ hadrons | | | | $h \to$ hadrons | | | |
| | $Z \to q\bar{q}$ | | | | $Z \to \nu\bar{\nu}$ | | | |
| $m_h$ (GeV) | $N_D$ | $N_B$ | $N_S$ | $\varepsilon$ (%) | $N_D$ | $N_B$ | $N_S$ | $\varepsilon$ (%) |
| 60 | 1356 | 1336 | 172 | 43 | 40 | 33.1 | 48.8 | 63 |
| 70 | 1363 | 1295 | 122 | 43 | 89 | 84.0 | 40.6 | 60 |
| 80 | 938 | 966 | 104 | 45 | 209 | 201 | 32.2 | 56 |
| 90 | 584 | 585 | 71.2 | 45 | 183 | 181 | 21.6 | 53 |
| 100 | 360 | 355 | 39.9 | 46 | 74 | 69.9 | 12.2 | 50 |
| 110 | 126 | 127 | 11.8 | 46 | 18 | 16.4 | 3.5 | 48 |
| | $h \to$ hadrons | | | | | | | |
| | $Z \to \ell^+\ell^-$ | | | | Combined | | | |
| $m_h$ (GeV) | $N_D$ | $N_B$ | $N_S$ | $\varepsilon$ (%) | $N_D$ | $N_B$ | $N_S$ | |
| 60 | 49 | 49.4 | 28.2 | 49 | 1445 | 1419 | 249 | |
| 70 | 43 | 52.8 | 24.1 | 50 | 1495 | 1432 | 187 | |
| 80 | 61 | 63.2 | 19.2 | 51 | 1208 | 1230 | 155 | |
| 90 | 56 | 61.3 | 13.0 | 50 | 823 | 827 | 106 | |
| 100 | 24 | 18.4 | 5.8 | 47 | 458 | 443 | 57.9 | |
| 110 | 3 | 4.2 | 1.6 | 42 | 147 | 148 | 16.9 | |

Table 3: Numbers of selected candidates, $N_D$, expected background events, $N_B$, and expected signal events, $N_S$, for different $m_h$ hypotheses in the $e^+e^- \to hZ$ search. The selection efficiencies, $\varepsilon$, are also given. The numbers of signal events are quoted for the h decay mode corresponding to the lowest efficiency and are computed assuming $\xi^2 \times B(h \to \text{hadrons}) = 1$. Only events with a signal over background ratio greater than 0.05 are considered.

10

| e+e− → hA | | | | |
|---|---|---|---|---|
| $(m_{\mathrm{h}}, m_{\mathrm{A}})$ (GeV) | $N_D$ | $N_B$ | $N_S$ | $\varepsilon$ (%) |
| (50,50) | 114 | 110 | 84.4 | 41 |
| (50,70) | 220 | 211 | 56.2 | 36 |
| (50,90) | 223 | 239 | 29.2 | 28 |
| (70,70) | 244 | 223 | 39.9 | 40 |
| (70,90) | 96 | 95.8 | 5.7 | 11 |
| (90,90) | 10 | 11.4 | 0.6 | 4 |

Table 4: Number of selected candidates, $N_D$, expected background events, $N_B$, and expected signal events, $N_S$, and selection efficiencies, $\varepsilon$, for different $(m_{\mathrm{h}}, m_{\mathrm{A}})$ hypotheses in the e+e− → hA search. The numbers of signal events are quoted for the h and A decay modes corresponding to the lowest efficiencies and are computed assuming $\eta^2 \times \mathrm{B}(\mathrm{h} \to \mathrm{hadrons}) = 1$. Only events with a signal over background ratio greater than 0.05 are considered.
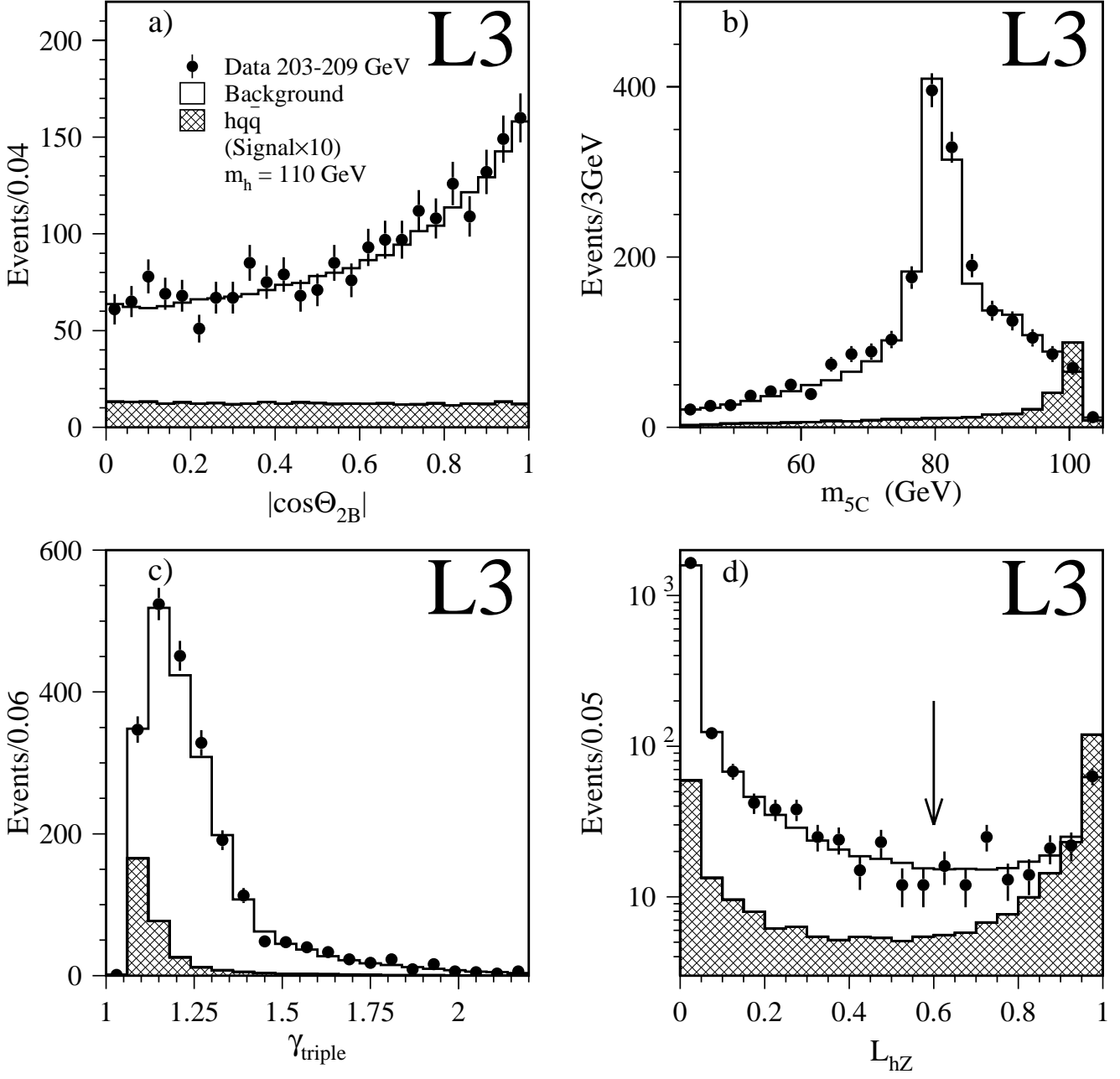
Figure 1: Distributions for the $e^+e^- \to hZ$ search in the four-jet final state of a) $|\cos\Theta_{2B}|$, b) $m_{5C}$, c) $\gamma_{triple}$, d) $L_{hZ}$. The points indicate data collected at $\sqrt{s} > 203$ GeV, the open histograms represent the expected background and the hatched histograms stand for a $m_h = 110$ GeV signal expected for $\xi^2 \times B(h \to hadrons) = 1$, multiplied by a factor of 10. The arrow in d) indicates the position of the cut.
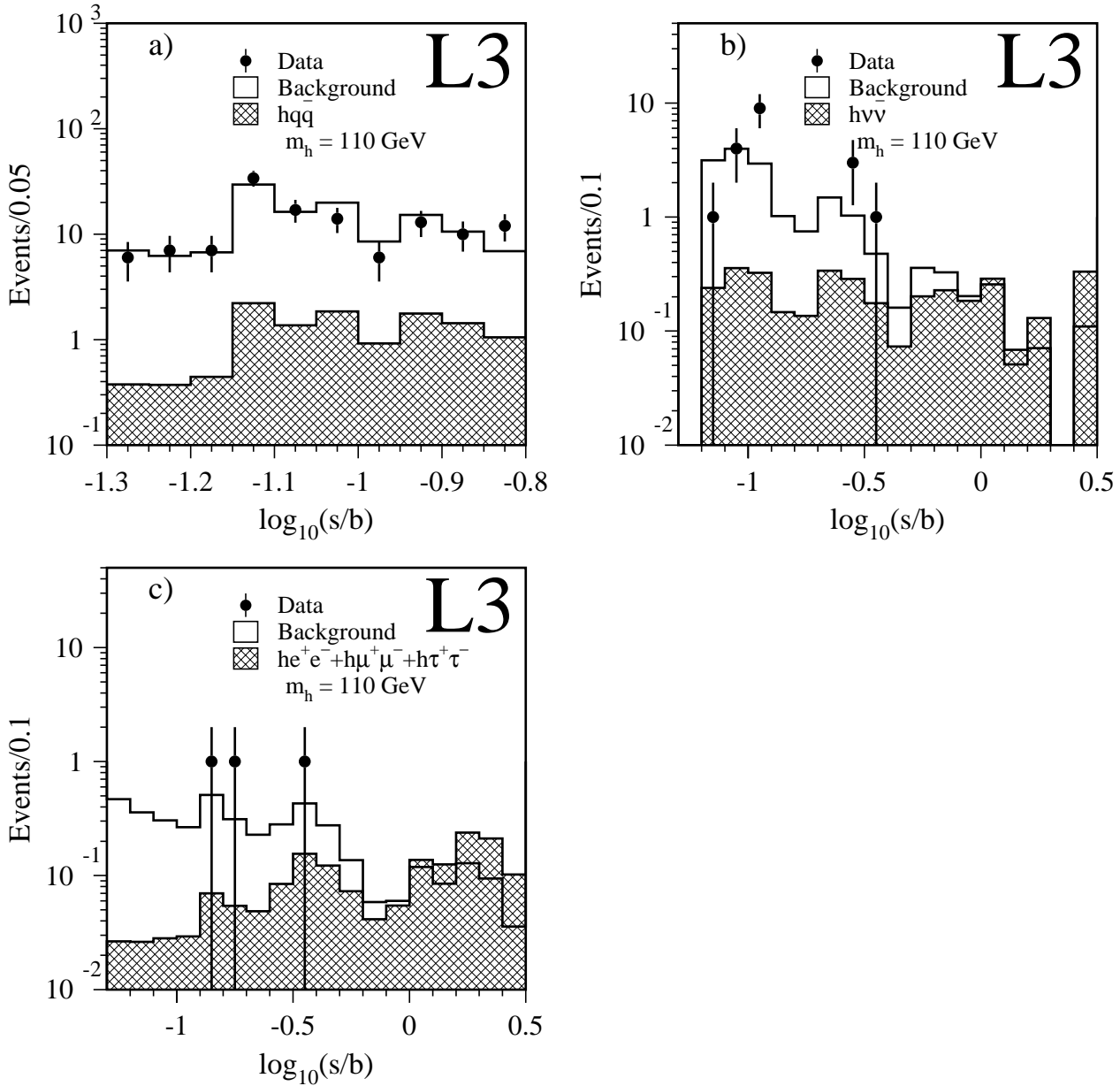
Figure 2: Distributions of the signal over background ratio for events selected in the $e^+e^- \to hZ$ search by the a) four-jet, b) two jets and missing energy and c) two jets and two lepton analyses. The points indicate data collected at $\sqrt{s} > 203$ GeV, the open histograms represent the expected background and the hatched histograms stand for a $m_h = 110$ GeV signal expected for $\xi^2 \times B(h \to \text{hadrons}) = 1$. Only events with $s/b > 0.05$ are shown.
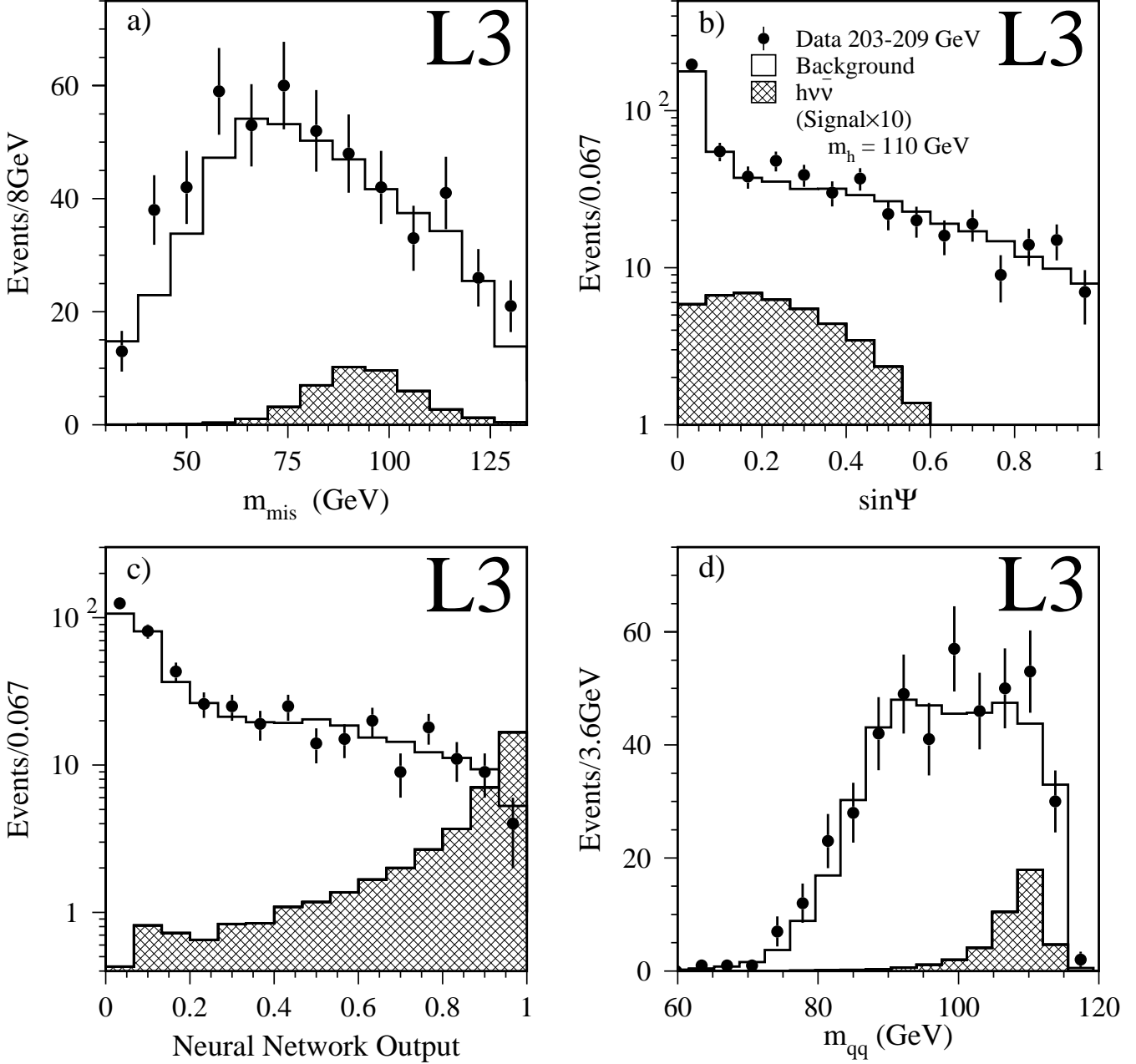
Figure 3: Distributions for the $e^+e^- \to hZ$ search in the two jet and missing energy final state of a) $m_{mis}$, b) $\sin \Psi$, c) neural network output and d) $m_{qq}$. The points indicate data collected at $\sqrt{s} > 203$ GeV, the open histograms represent the expected background and the hatched histograms stand for a $m_h = 110$ GeV signal expected for $\xi^2 \times B(h \to hadrons) = 1$, multiplied by a factor of 10.
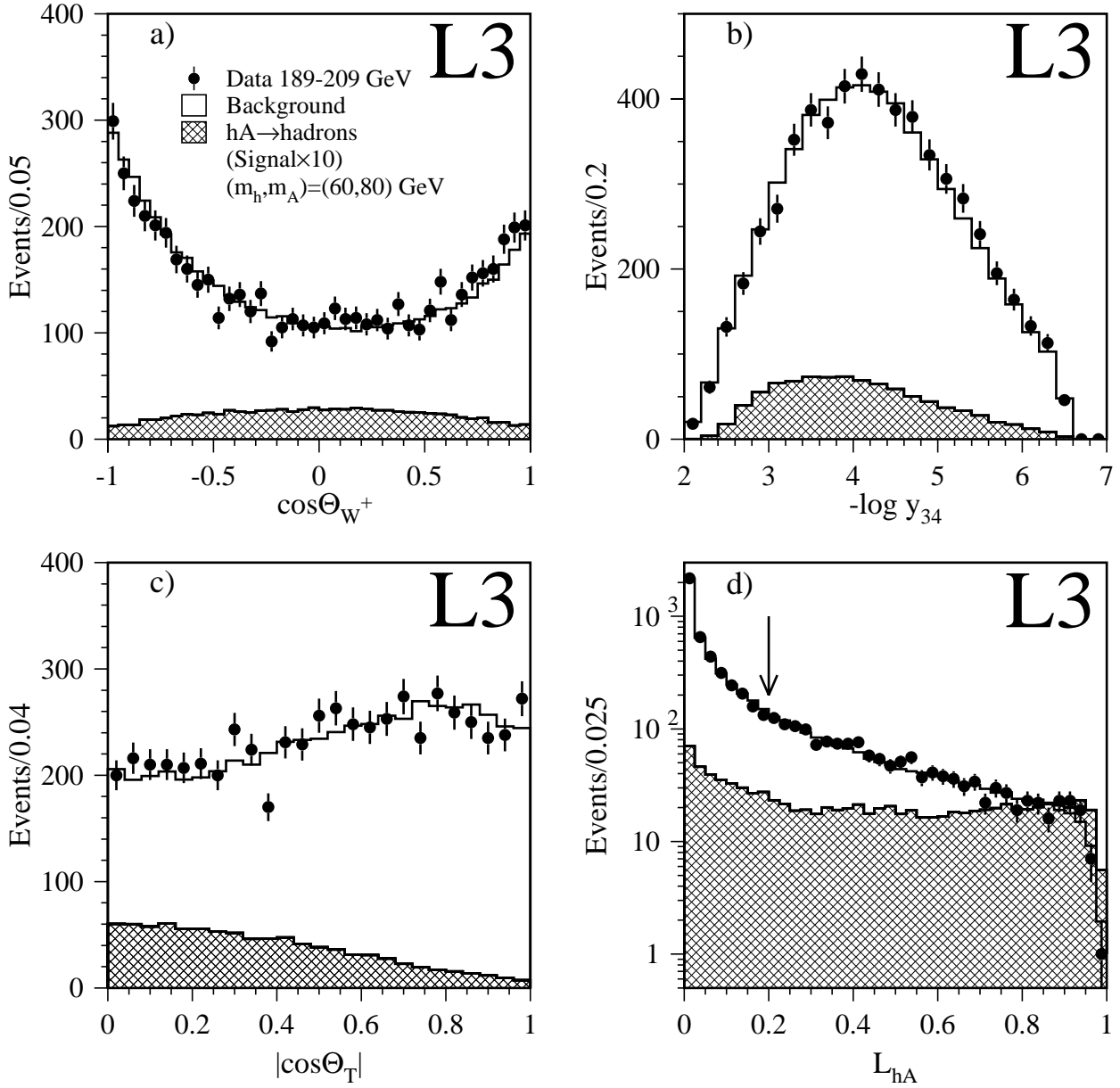
Figure 4: Distributions for the $e^+e^- \rightarrow hA$ search of: a) $\cos\Theta_{W^+}$, b) $-\log y_{34}$, c) $|\cos\Theta_T|$, d) $L_{hA}$. The points indicate the data, the open histograms represent the expected background and the hatched histograms stand for a $(m_h, m_A) = (60, 80)$ GeV signal expected for $\eta^2 \times B(hA \rightarrow \text{hadrons}) = 1$, multiplied by a factor of 10. The arrow in d) indicates the position of the cut.
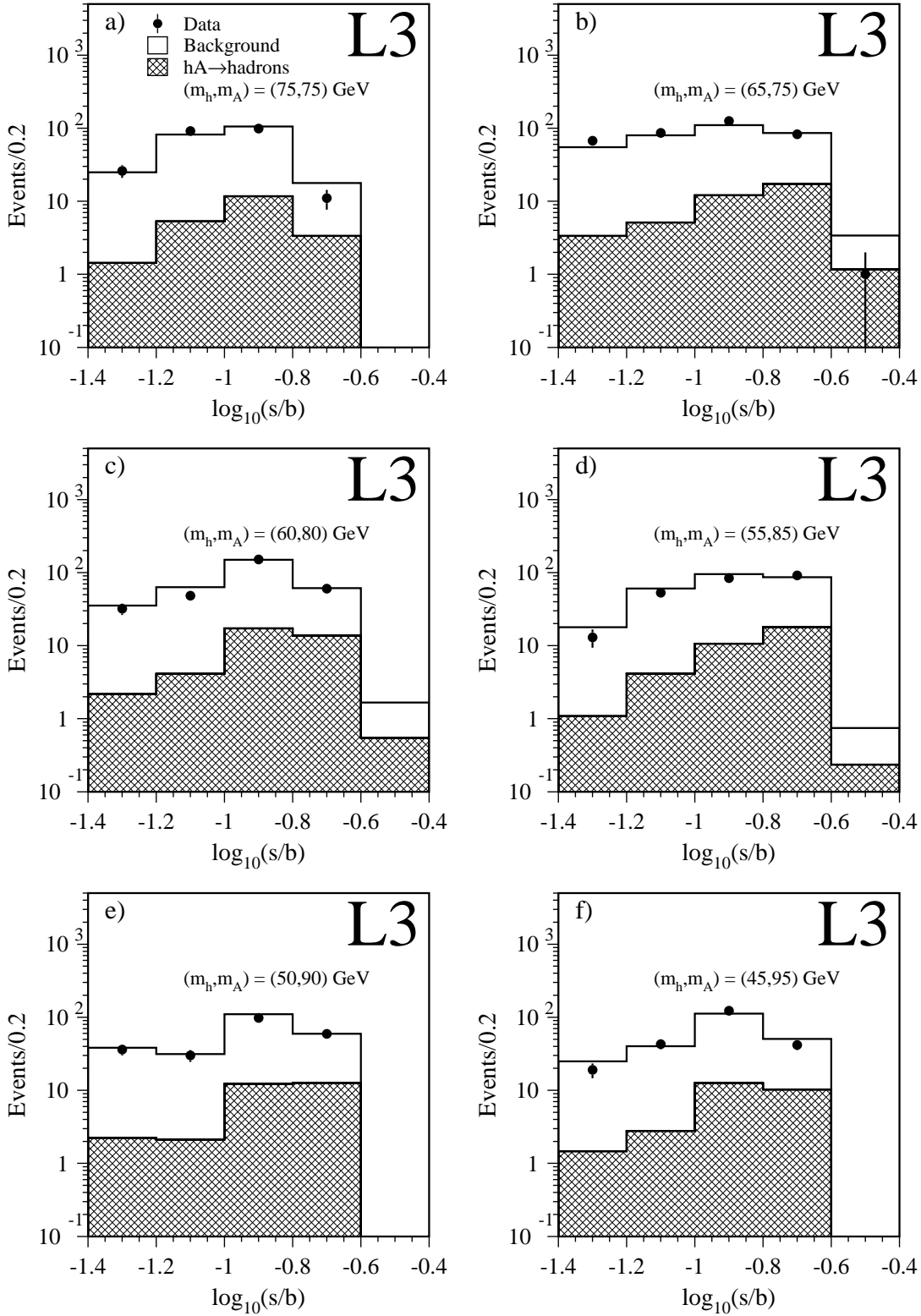
Figure 5: Distributions of the signal over background ratio for events selected by the $e^+e^- \to hA$ search for different $(m_h, m_A)$ mass hypotheses: a) (75,75) GeV, b) (65,75) GeV, c) (60,80) GeV, d) (55,85) GeV, e) (50,90) GeV and f) (45,95) GeV. The points indicate the data, the open histograms represent the expected background and the hatched histograms stand for a signal of the given $(m_h, m_A)$ hypothesis expected for $\eta^2 \times B(hA \to hadrons) = 1$.
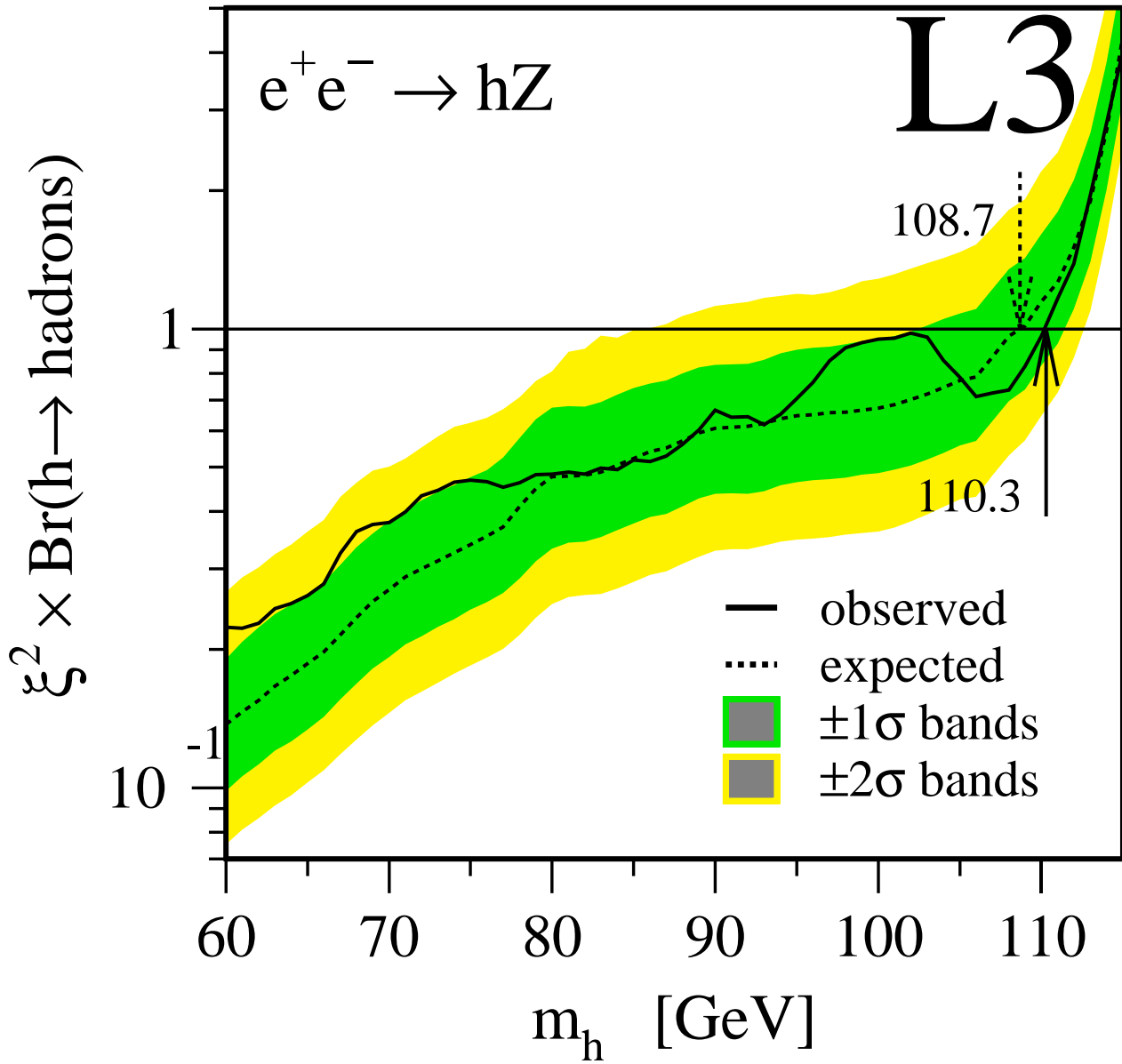
Figure 6: The 95% confidence level upper limit on $\xi^2 \times \mathrm{Br}(h \to \mathrm{hadrons})$ as a function of $m_h$. The solid line indicates the observed limit and the dashed line stands for the median expected limit. The shaded areas show the $1\sigma$ and $2\sigma$ intervals centered on the median expected limit. The observed and expected limits on $m_h$ for $\xi^2 \times \mathrm{Br}(h \to \mathrm{hadrons}) = 1$ are also shown.
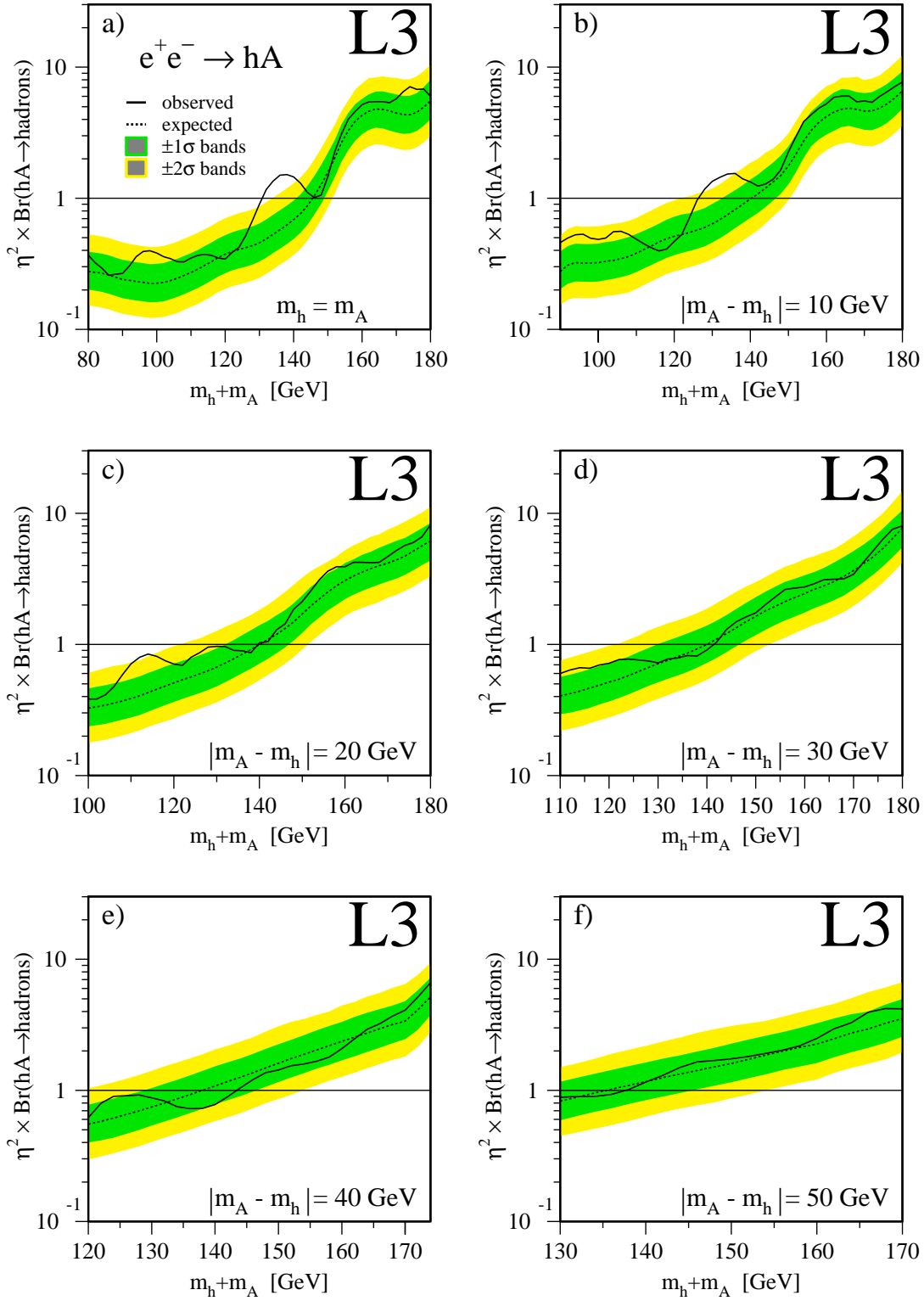
Figure 7: The 95% confidence level upper limit on the quantity $\eta^2 \times \mathrm{Br}(hA \to \text{hadrons})$ as a function of $m_h + m_A$ for different values of the difference: $|m_A - m_h|$: a) 0 GeV, b) 10 GeV, c) 20 GeV, d) 30 GeV, e) 40 GeV and f) 50 GeV. The solid lines indicate the observed limits and the dashed lines stand for the median expected limits. The shaded areas show the $1\sigma$ and $2\sigma$ intervals centered on the median expected limits.